Braz J Phys (2012) 42:323–329
DOI 10.1007/s13538-012-0095-9

ATOMIC PHYSICS

Photoionization Microscopy of Rydberg Hydrogen Atom in a Generalized van der Waals Potential

De-hua Wang · Tian-tian Tang · Li-jie Tian

Received: 9 May 2011 / Published online: 24 August 2012

Abstract The ionization dynamics of a Rydberg hydrogen atom in a generalized van der Waals potential is studied using a semiclassical analysis of photoionization microscopy. Interference patterns of the 2-D radial probability density of the electrons escaping from a photoionization process have been calculated to simulate the patterns recorded on a position-sensitive detector. The added contributions from different ionization trajectories from the atom to the detector generate the interference pattern. The interference pattern is sensitive to one of the parameters governing the electron motion in the generalized van der Waals potential. The photoionization microscopy pattern can therefore be controlled by changes in the external potential.

Keywords Photoionization microscopy · Rydberg atom · van der Waals potential · Probability density

1 Introduction

In the last two decades, many authors have discussed the photoionization or photoabsorption of Rydberg atoms in external fields in great detail, both theoretically and experimentally [1–5]. The photoabsorption spectra of Rydberg atoms in external fields display oscillations. The oscillatory structure is a quantum effect, caused by the interference between the initial and the final state wave functions [6]. The oscillatory photoabsorption spectra are therefore manifestations of the wave-function oscillations, which had been very difficult to observe in atomic systems until brought to light by the development of photoelectron imaging.

Photoelectron imaging, a form of microscopy, was introduced in the early 1980s by Demkov et al., who laid its theoretical foundations and proposed an experiment in which an atom would be photoionized by an electric field [7–9]. In 2002, Nicole et al. carried out the first photoionization microscopy experiment [10]. They observed a geometrical interference pattern when photoelectrons were ejected from a Rydberg Xe atom. The observed pattern was explained by the semiclassical theory of Bordas et al. [11, 12], their numerical simulation showing good agreement with the experimental data. By contrast with the photodetachment microscopy of negative ions in electric fields, in which only two trajectories interfere at a given point on a detector [13], in the photoionization of a Rydberg atom in an electric field an infinite number of electron trajectories contribute to the interference pattern, an effect due to the long-range Coulomb attraction between the excited electron and the atomic core. The coexistence of the Coulomb and the electric field potentials leads to complex motion of the excited electron. To simulate the electronic movement, Zhao and Delos developed a semiclassical open-orbit theory and studied the photoionization microscopy of a Rydberg hydrogen atom in an electric field [14]. Their semiclassical theory, which incorporates Maslov indices and corrects the singularities arising in semiclassical computations of the wave functions, is more complete than the approach of Bordas et al. [11, 12]. Subsequently, Wang and Liu et al. studied the photoionization microscopy of Rydberg hydrogen atoms in parallel electric and magnetic fields [15]. The magnetic field gives rise to remarkably complex interference patterns.

Recently, with the advancement of surface physics, the dynamics of the Rydberg atoms near metal surfaces has

D.-h. Wang (✉) · T.-t. Tang · L.-j. Tian
College of Physics and Optoelectronic Engineering,
Ludong University,
Yantai 264025, China
e-mail: jnwdh@sohu.com

attracted much attention [16–21]. For highly excited Rydberg atoms, the outer electron has a very low characteristic frequency in comparison with the electronic frequencies in the metal. The atom–metal interaction is therefore well described by the image potential method [18, 21]. If the (infinitely heavy) hydrogen nucleus is at the origin of the coordinate system and the metal surface, at the $z=-$d plane, in atomic units, the electrostatic image potential between the excited electron and the metal surface has the form

$$V_{im} = \frac{1}{\sqrt{\rho^2 + (2d+z)^2}} - \frac{1}{4(d+z)}.$$

If the distance d between a single hydrogen atom and the metal surface is much larger than the atomic radius r, the binomial expansion of the electrostatic image potential can be stopped at the quadratic term, to yield the so-called instantaneous van der Waals potential between the excited electron and the metal surface [16, 18, 22]:

$$V_{ivp} = -\frac{1}{16d^3}\left(x^2 + y^2 + 2z^2\right). \quad (1)$$

The generalized van der Waals interaction is defined by the equality [23]

$$V = \gamma\left(x^2 + y^2 + \beta^2 z^2\right), \quad (2)$$

where γ and β are constants.

The van der Waals force is important in numerous areas of solid-state physics, biology, and chemistry. It is particularly important in the study of cold, neutral atoms close to micro- or nanoscaled bodies [24–30]. The chaotic dynamics of a hydrogen atom in the generalized van der Waals potential has been investigated by many authors [31–33]. Very recently, Yang and Liu et al. studied the ionization of a Rydberg hydrogen atom near a metal surface with a semiclassical analysis of photoionization microscopy [34]. The ionization dynamics of a Rydberg atom in the generalized van der Waals potential has nonetheless never been studied. In this paper, we carry out a semiclassical analysis of photoionization microscopy for a Rydberg atom in a generalized van der Waals potential. Our results indicate that photoionization microscopy can be controlled by changing the parameters of the generalized van der Waals potential, a conclusion that may guide experimental photoionization microscopy studies in the future.

2 Theory

While the hydrogen atom Hamiltonian is integrable, the problem of a hydrogen atom in a generalized van der Waals potential poses a more difficult mathematical challenge. Semiclassical treatment of the atom in the van der Waals potential is nonetheless expected to describe the physics of the system. Under continuous laser radiation, the hydrogen atom is excited from the ground or a low excited state to a high Rydberg state. The absorption of a photon creates an electronic wave near the atom, which propagates outwards in all directions. In the semiclassical description, the propagation is associated with outgoing classical trajectories, determined by the classical Hamiltonian canonical equations. Under the influence of the Coulomb attractive potential and van der Waals potential, the electrons traveling along a few of the outgoing trajectories escape the atom; the waves then propagate to a distant position-sensitive detector. Whenever two or more electron trajectories reach the same point on the detector, the corresponding waves interfere constructively or destructively, giving rise to an observable interference pattern on the detector.

Let r be the distance between the electron and the hydrogen nucleus. The potential is then the sum of the attractive Coulomb and generalized van der Waals potentials. The Hamiltonian of this system can be written in the form [31]:

$$H = \frac{p_\rho^2}{2} + \frac{p_z^2}{2} + \frac{p_\phi^2}{2\rho^2} - \frac{1}{\sqrt{\rho^2+z^2}} + \gamma\left(\rho^2 + \beta^2 z^2\right), \quad (3)$$

in cylindrical coordinates and units such that $e = h = m_e = 1$.

Given the cylindrical symmetry, the z component $l_z=p_\phi$ of the angular momentum is conserved, and the motion along the ϕ coordinate is separated from the movement in the (ρ, z) plane. Here, we consider the case $p_\phi=0$, which leaves two degrees of freedom.

Even this reduced problem presents difficulties. Most obvious among these is the Coulomb singularity at $\rho^2 + z^2 = 0$ on the right-hand side of Eq. (3). To make it treatable, we introduce a regularized transformation to semi-parabolic coordinates (u,v) [35], where $\rho=uv$, $z = (u^2 - v^2)/2$, and the conjugate momenta $p_u = du/d\tau, p_v = dv/d\tau$ are defined with respect to a rescaled time τ given by the equality $\frac{d\tau}{dt} = \frac{1}{u^2+v^2}$.

The resulting regularized Hamiltonian has the form [31]

$$h = \tfrac{1}{2}\left(p_u^2 + p_v^2\right) - E(u^2+v^2) + A(u^6+v^6) + B(u^4v^2 + u^2v^4) = 2, \quad (4)$$

where $A = \left(\gamma\beta^2\right)/4, B = \gamma - \left(\gamma\beta^2\right)/4$.

In Eq. (4), the true energy E is a parameter, and the physical trajectories evolve in an effective potential whose

pseudo-energy is always equal to 2. This regularized transformation diminishes the Coulomb singularity. The equations of motion associated with h(u,v) are:

$$\begin{cases} \ddot{u} = 2Eu - 6Au^5 - B(4u^3v^2 + 2uv^4) \\ \ddot{v} = 2Ev - 6Av^5 - B(4u^2v^3 + 2u^4v) \end{cases} . \quad (5)$$

Suppose the electron in the excited state is isotropically ejected from the origin with an outgoing angle θ between its initial velocity and the z-axis, and energy $E = -1.0 \times 10^{-8}$ a.u. and reaches the detector located at $z = -|z_{\text{det}}|$. Integration of the Hamiltonian motion equations with the initial conditions ρ=0 and z=0 determines the trajectories reaching the detector surface within a maximum time T_0. If this evolution time is increased, more trajectories can hit the detector, and the calculation becomes more demanding. In practice, therefore, the evolution time must be limited, and we choose T_0=20 (arbitrary units). The number of photoelectron trajectories through a given point on the detector surface is great. When a trajectory reaches the detector, we record the final value of the cylindrical coordinate $\rho_i(\theta_i)$.

Next, with the semiclassical approximation, we compute the wave function at each point $\rho_i(\theta_i)$. The semiclassical wave function $\psi_i(\rho_i)$ for the ith trajectory depends on its classical density A_i and classical action function S_i [15]:

$$\psi_i(\rho_i) = \sqrt{A_i}\exp\left(iS_i - \frac{\pi}{2}\mu_i\right) . \quad (6)$$

Here, the action $S_i = \int p_i dq_i$. The symbol μ_i denotes the Maslov index, equal to the number of singularity points traversed by the electron trajectory. The classical density A_i is defined as

$$A_i = \frac{d\theta_i}{d\rho_i}\sin\theta_i . \quad (7)$$

For a given point on the detector, we compute several trajectories through it. The resulting wave function is the sum of the wave functions $\psi_i(\rho_i)$ along the trajectory i from the electron source to this point [15]:

$$\psi_{sc}(\rho) = \sum_i \psi_i(\rho_i) = \sum_i \sqrt{A_i}\exp\left(iS_i - \frac{\pi}{2}\mu_i\right) . \quad (8)$$

The radial probability density on the detector is then determined from the expression

$$P(\rho, z_{\text{det}}, \varphi) = |\psi_{sc}(\rho)|^2 = \sum_i A_i + 2\sum_{i<j}\sqrt{A_iA_j}\cos\left[S_i - S_j - \tfrac{\pi}{2}\left(\mu_i - \mu_j\right)\right] . \quad (9)$$

The first term in the above formula is the classical probability density distribution, and the second one represents the interference among different classical paths reaching each point on the detector [15].

3 Computational Results and Discussion

In all our computations, the generalized van der Waals potential is attractive, i.e., $\gamma = A + B > 0$. The energy of the Rydberg hydrogen atom is $E = -1.0 \times 10^{-8}$ a.u., and the detector is located at $z = -|z_{\text{det}}| = -1.0$ (arbitrary unit). We keep the parameter A unchanged (A=1/6) and show how the parameter B in the generalized van der Waals potential affects the spatial distributions of the electronic wave function. Figure 1 plots a

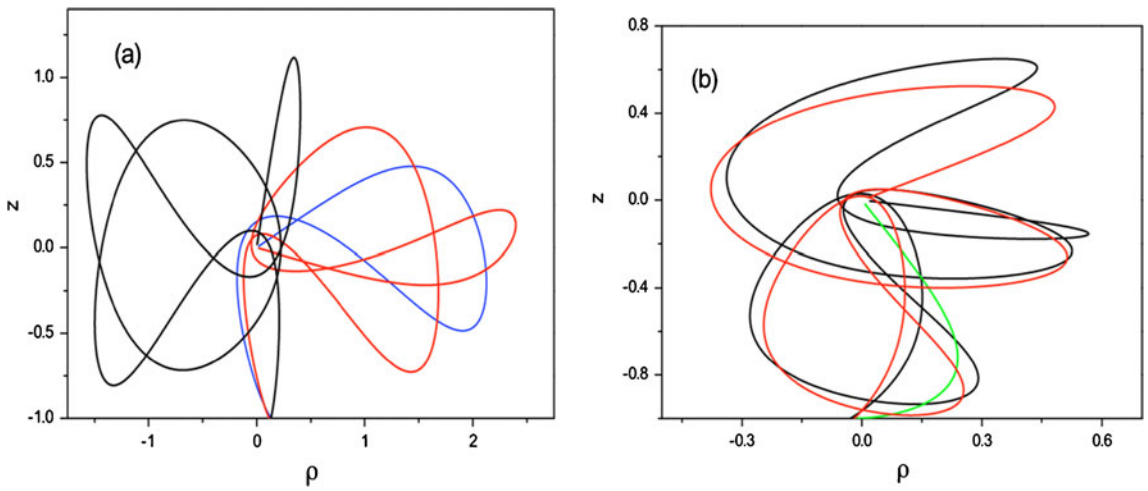

Fig. 1 (Color online) Some classical trajectories of the photoelectron in a generalized van der Waals potential hitting the detector at the point. Different trajectories are represented by different colors. **a** B=−0.1, ρ=0.13, z=−1.0; **b** B=5.0, ρ=−0.02, z=−1.0

few classical photoelectron trajectories hitting the detector at a given point. Although ρ is positive, to display the trajectories more clearly, we have expanded it to negative values. Figure 1a depicts trajectories with B=−0.1, which encircle the nucleus along the ρ-axis one or more times before reaching the detector. In Fig. 1b, with B=5.0, the trajectories encircle the nucleus along the z-axis once or more than once before hitting the detector. This can be interpreted as follows: for given parameter A=1/6, the second term in the generalized van der Waals potential governing the motion along the z-direction is fixed $\gamma\beta^2 = 4A = 2/3$. With B=−0.1, we have $\gamma = \frac{1}{15} < \gamma\beta^2$. Therefore, the attractive potential in the generalized van der Waals potential along the z-direction is stronger than the one along the ρ-direction, and the trajectory will encircle the nucleus along the ρ-axis many times before hitting the detector. With B=5.0, by contrast, $\gamma = \frac{31}{6} > \gamma\beta^2$, making the attractive potential along the ρ-direction stronger than the potential along the z-direction. The trajectory will therefore encircle the nucleus along the z-axis many times before striking the detector.

Next, we study the evolution of the final position ρ_i at the detector as a function of the ejection angle θ_i. We let B vary in the range (−0.15, 10.0). As explained by Ganesan et al. [31], the system is integrable for three special conditions: B=0, B=3A, and B=15A. In our study of chaotic ionization, with A=1/6, the special values are B=0, 0.5, and 2.5. Accordingly, we split the range of B parameters into four segments: B=(−0.15, 0.0), (0.0, 0.5), (0.5, 2.5), (2.5, 10.0). The results are shown in Figs. 2, 3, 4, and 5. In all computations, adjacent points in the θ grid are separated by 0.001 rad. Figure 2 shows the θ–ρ curve with B in the range (−0.15, 0.0). In Fig. 2a, with B=−0.15, the θ–ρ curve is very complex. Infinite trajectories reach a given point on the detector surface. As the ejection angle θ is varied between π and 2.606, the electrons move toward the detector and hit it before crossing the negative z-axis. These trajectories are called direct trajectories [10]. For smaller θ, the electron crosses the negative z-axis and then encircles the nucleus one or more times before hitting the detector. These trajectories are called indirect trajectories [10]. For larger B, the strong attractive potential in the ρ-direction restricts the electron motion in the plane perpendicular to the z-axis. The maximum attainable ρ on the detector surface is reduced, and the θ–ρ curve becomes simpler, as in Fig. 2b. In Fig. 2c, with B=−0.005, close to the integrable case B=0,

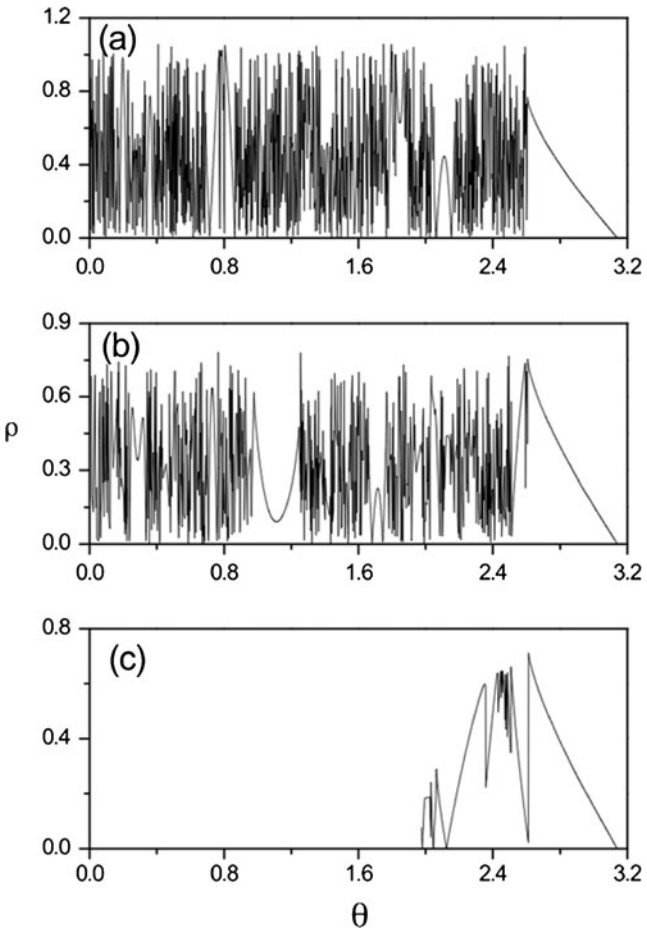

Fig. 2 Final radial distance ρ as a function of the ejection angle θ. **a** B=−0.15, **b** B=−0.1, **c** B=−0.005

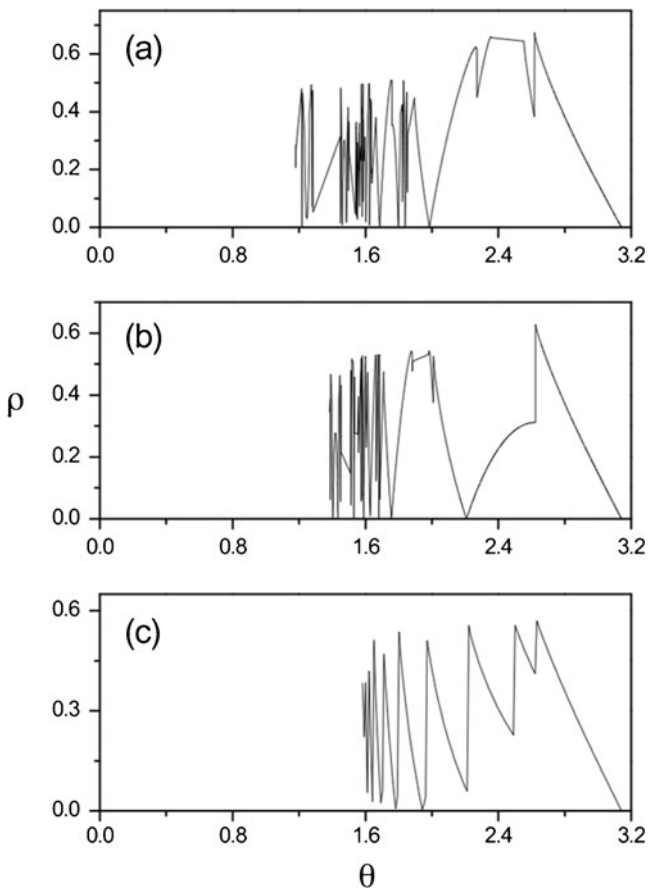

Fig. 3 Final radial distance ρ as a function of the ejection angle θ. **a** B=0.1, **b** B=0.25, **c** B=0.45

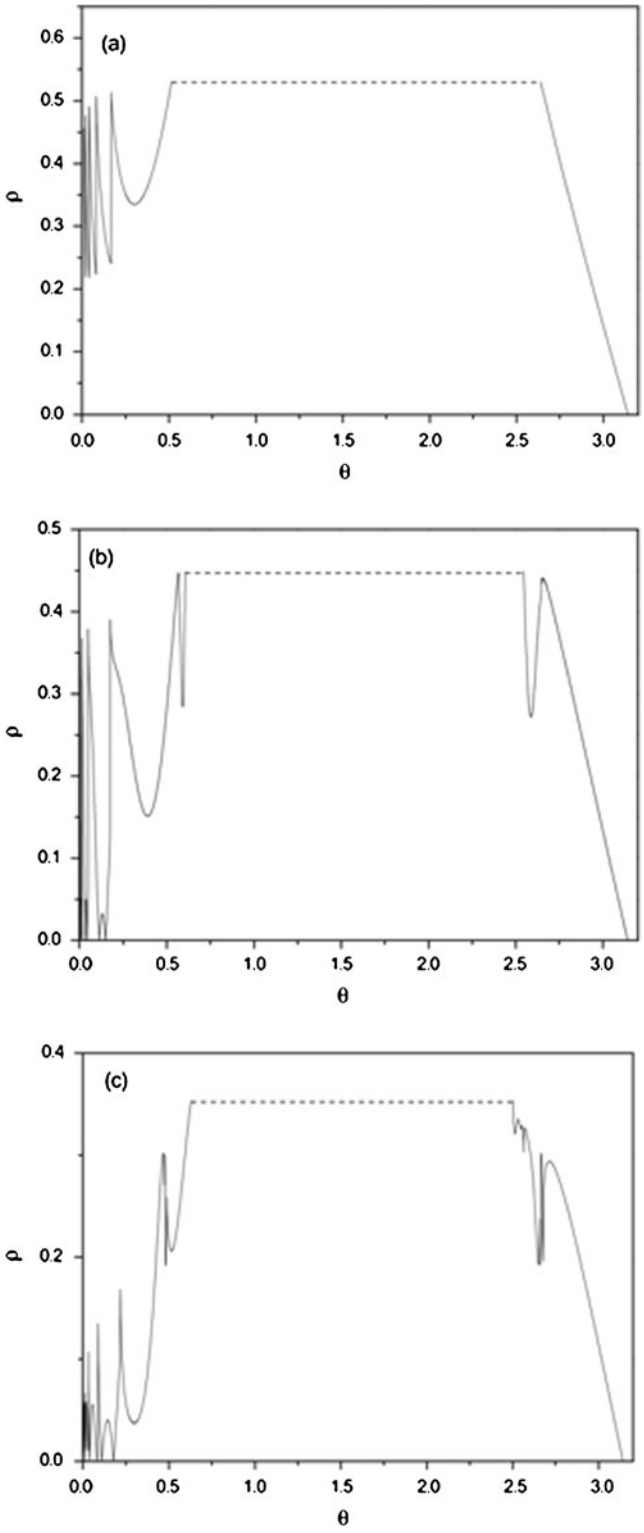

Fig. 4 Final radial distance ρ as a function of the ejection angle θ. **a** B=0.6, **b** B=1.0, **c** B=2.0

fewer trajectories can reach the detector surface, and the θ–ρ curve becomes much simpler. By contrast with the previous cases, only a limited number of trajectories can now reach the detector.

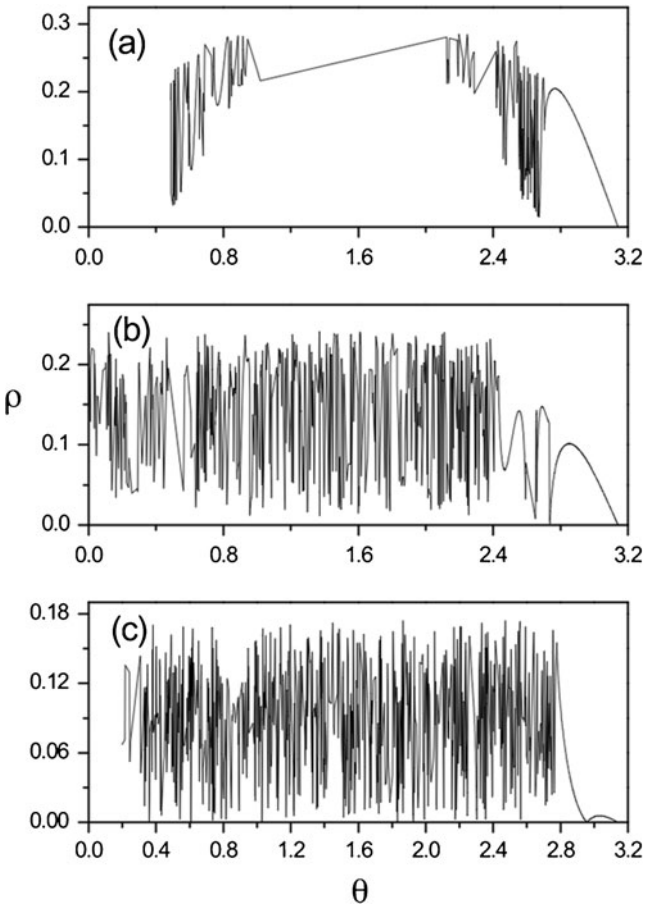

Fig. 5 Final radial distance ρ as a function of the ejection angle θ. **a** B=3.5, **b** B=5.0, **c** B=10.0

As B becomes positive, chaotic behavior is reinstated. The number of the trajectories reaching the detector surface grows, and the θ–ρ curve becomes complex once again. Subpanels a and b of Fig. 3 show examples. With B=0.45, very close to the second integrable point (B=0.5), the θ–ρ curve is again simplified. Figure 4 shows θ–ρ curves in the third chaotic range, B=(0.5, 2.5). In Figure 4a, with B=0.6, the curve can be split into two segments: θ=(π, 2.64) and θ=(0.58, 0.03). In the first segment, the main contribution to the curve comes from the direct trajectories. In the second region, by contrast, the indirect trajectories are important. The electron encircles the nucleus several times before hitting the detector surface. The number of the indirect trajectories contributing to the θ–ρ curve grows with B, as shown by Fig. 4b and c. Figure 5 shows the θ–ρ curve in the fourth chaotic region B=(3.5, 10.0). Here, the large B parameter makes the attractive potential in the ρ-direction stronger than the potential in the z-direction and further restricts the motion of the electron in the plane perpendicular to the z-axis. The maximum attainable position on the detector surface is progressively diminished as B grows. Following ejection from the nucleus, the electron hits the

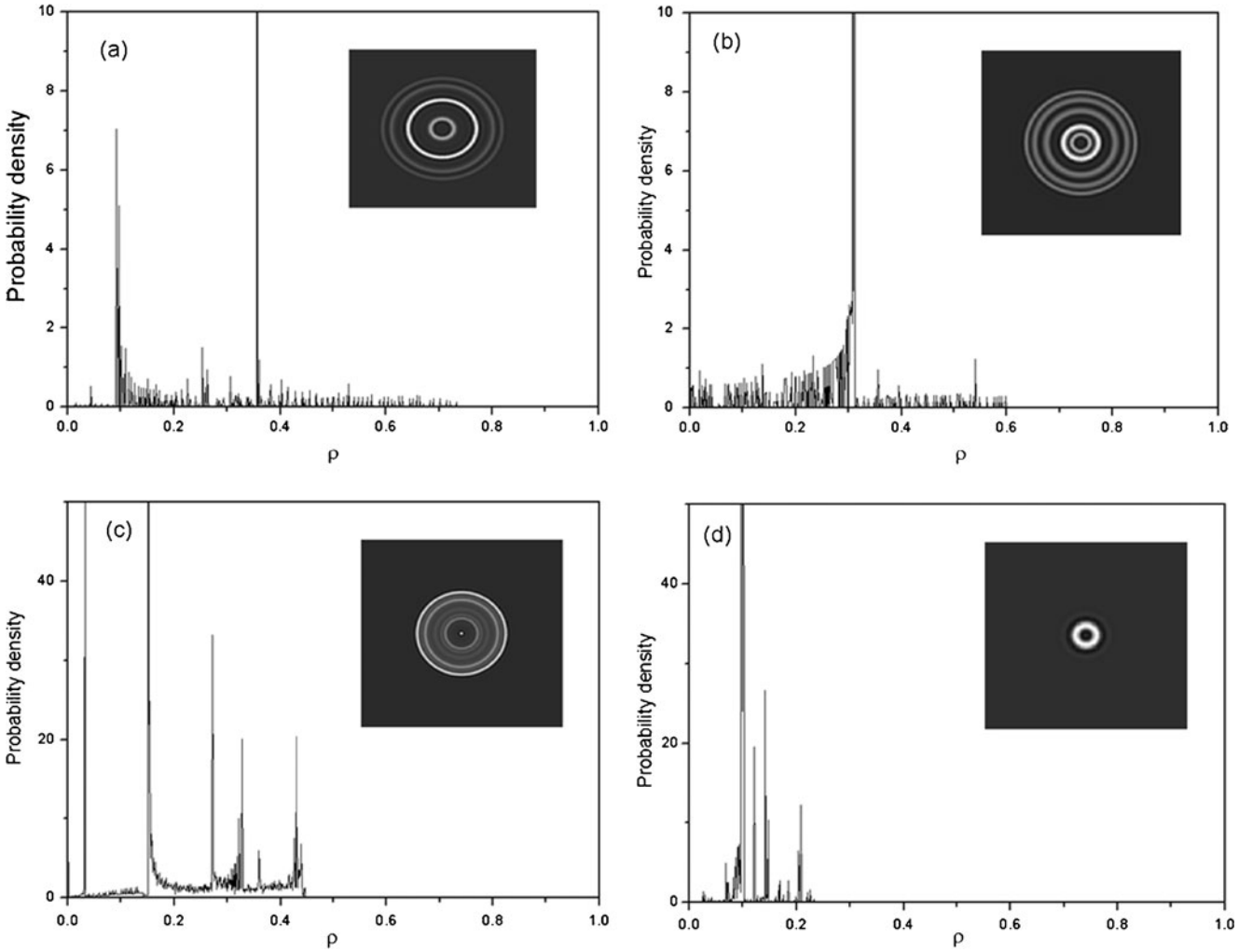

Fig. 6 Radial probability density distributions and their 3-D contour plots of the photoelectron in a generalized van der Waals potential; the parameter B is varied from −0.1 to 10.0. **a** B=−0.1, **b** B=0.25, **c** B=1.0, **d** B=5.0. The contour plots are given in the *inset* of each plot

detector surface in a short time, and the θ–ρ plot becomes much more complex. Overall, from Figs. 2, 3, 4, and 5, the number of chaotic ionization trajectories is large, and the θ–ρ plot, complex for B<0 and for B>2.5. In the intermediate region, the number of the chaotic ionization trajectories is small and the θ–ρ curve, relatively simple.

To display the electron distribution on the detector surface, we have calculated the radial probability–density distribution for the electrons. From the results in Figs. 2, 3, 4, and 5, we expect the distribution to depend on the parameter B in the generalized van der Waals potential. Figure 6 shows radial probability–density distributions and their 3-D contour plots for B's varying from −0.1 to 5.0. The radial distribution displays a clear interference pattern, the contour plots showing a sequence of interference fringes. Figure 6a depicts the probability density distribution with B=−0.1. Under this condition, the number of the trajectories reaching the detector surface is very large, and the electron probability distribution is widely spread out, the radius of the outermost ring in the contour plot being relatively large. For growing parameter B, the electron probability–density distribution narrows, and the disk in the contour plot shrinks. With B=0.25, for example, the maximum position the electron can reach on the detector plane is ρ_{max}=0.63, with B=1.0, ρ_{max}=0.44. With B=5.0, the cyclotron motion in the ρ-direction is so strong that the electron becomes restricted to a small region near the nucleus, with very small ρ_{max}. Under this condition, the contour plot is reduced to a small circle.

4 Conclusion

In summary, we have carried out a semiclassical analysis of the ionization dynamics of a Rydberg hydrogen atom in a generalized van der Waals potential, a model of photoionization microscopy. We have computed the radial probability–density distribution for the electrons and present contour

plots to simulate the pattern imprinted on a position-sensitive detector. The oscillatory patterns in the probability–density distribution reflect the interference among various classical electronic trajectories running from the atom to the plane of the detection.

We have found that the interference pattern in the photoelectron probability density is sensitive to the parameters in the generalized van der Waals potential. The photoionization microscopy pattern is therefore controlled by the parameters in the external potential. Our calculations of the wave function and probability–density distribution relied on the semiclassical approximation. Our plans include future exact quantum mechanical calculations to be compared with the above discussed results. To our knowledge, no photoionization microscopy experiments in systems that can be realistically modeled by a Rydberg atom in a generalized van der Waals potential have been reported. Since our calculations show that such systems are amenable to semiclassical treatment, we hope that this study will guide future experimental studies of the photoionization microscopy in such systems.

Acknowledgments This work was supported by the National Natural Science Foundation of China (grant nos. 11074104 and 10604045) and the Higher Educational Science and Technology Program of Shandong Province, China (grant no. J09LA02). We also thank the referee's good suggestions.

References

1. P.M. Koch, K.A.H. Van Leeuwen, Phys. Rep. **255**, 290 (1995)
2. H. Hasegawa, M. Robnik, G. Wunner, Prog. Theor. Phys. Suppl. **98**, 198 (1989)
3. M.L. Du, J.B. Delos, Phys. Rev. A **38**, 1896 (1988)
4. B. Hüpper, J. Main, G. Wunner, Phys. Rev. A **53**, 744 (1996)
5. N.S. Simonovic, J. Phys, B: At. Mol Opt. Phys. **30**, L613 (1997)
6. M.L. Du, J.B. Delos, Phys. Rev. A **38**, 1913 (1988)
7. Y. Demkov, V. Kondratovich, V. Ostrovskii, JETP Lett **34**, 403 (1982)
8. V.D. Kondratovich, V.N. Ostrovsky, J. Phys. B **17**, 1981 (1984)
9. V.D. Kondratovich, V.N. Ostrovsky, J. Phys. B **17**, 2011 (1984)
10. C. Nicole, H.L. Offerhaus, M.J.J. Vrakking, F. Lepine, C. Bordas, Phys. Rev. Lett. **88**, 133001 (2002)
11. C. Bordas, F. Lepine, C. Nicole, M.J.J. Vrakking, Phys. Rev. A **68**, 012709 (2003)
12. F. Lepine, C. Bordas, C. Nicole, M.J.J. Vrakking, Phys. Rev. A **70**, 033417 (2004)
13. M.L. Du, Phys. Rev. A **40**, 4983 (1989)
14. L.B. Zhao, J.B. Delos, Phys. Rev. A **81**, 053417 (2010)
15. L. Wang, H.F. Yang, X.J. Liu, H.P. Liu, M.S. Zhan, J.B. Delos, Phys. Rev. A **82**, 022514 (2010)
16. K. Ganesan, K.T. Taylor, J. Phys. B **29**, 1293 (1996)
17. P. Nordlander, Phys. Rev. B **53**, 4125 (1996)
18. N.S. Simonovic, Phys. Lett. A **331**, 60 (2004)
19. G.R. Lloyd, S.R. Procter, T.P. Softley, Phys. Rev. Lett. **95**, 133202 (2005)
20. G.R. Lloyd, S.R. Procter, E.A. McCormack, T.P. Softley, J. Chem. Phys. **126**, 184702 (2007)
21. D.H. Wang, M.L. Du, S.L. Lin, J. Phys. B **39**, 3529 (2006)
22. A. Landragin et al., Phys. Rev. Lett. **77**, 146 (1996)
23. Y. Alhassid, E.A. Hinds, D. Meschede, Phys. Rev. Lett. **59**, 1545 (1987)
24. T. Aoki, A.S. Parkins, D.J. Alton, C.A. Regal, B. Dayan, E. Ostby, K.J. Vahala, H.J. Kimble, Phys. Rev. Lett. **102**, 083601 (2009)
25. K.P. Nayak, K. Hakuta, New J. Phys. **10**, 053003 (2008)
26. V.G. Minogin, S. Nic Chormaic, Laser Phys. **20**, 32 (2010)
27. L. Russell, D.A. Gleeson, V.G. Minogin, S. Nic Chormaic, J. Phys. B: At. Mol. Opt. Phys. **42**, 185006 (2009)
28. M. Morrissey, K. Deasy, Y. Wu, S. Chakrabarti, S. Nic Chormaic, Rev. Sci. Instrum. **80**, 053102 (2009)
29. E. Vetsch, D. Reitz, G. Sague, R. Schmidt, S.T. Dawkins, A. Rauschenbeutel, Phys. Rev. Lett. **104**, 203603 (2010)
30. R. Schmidt, S.N. Chormaic, V.G. Minogin, J. Phys. B **44**, 015004 (2011)
31. K. Ganesan, M. Lakshmanan, Phys. Rev. A **42**, 3940 (1990)
32. D. Farrelly, J.E. Howard, Phys. Rev. A **48**, 851 (1993)
33. M. Inarrea, J.P. Salas, Phys. Rev. E **66**, 056614 (2002)
34. H.F. Yang, L. Wang, X.J. Liu, H.P. Liu, Chin. Phys.B **20**, 063203 (2011)
35. P.A. Dando, T.S. Monterio, D. Delande, K.T. Taylor, Phys. Rev. A **54**, 127 (1996)